



A new high-temperature plasma immersion ion implantation system with electron heating

R.M. Oliveira*, J.A.N. Gonçalves, M. Ueda, J.O. Rossi, P.N. Rizzo

INPE, Av. dos Astronautas, 1758. 12227-010, São José dos Campos, SP, Brazil

ARTICLE INFO

Available online 21 March 2010

Keywords:

Plasma immersion ion implantation
Oxide cathode
Ion diffusion

ABSTRACT

The temperature of the substrate has strong influence on the diffusion coefficient of nitrogen ions during plasma immersion ion implantation (PIII) performed in metallic surfaces, which affect the ion implantation profiles and can lead to the formation of thick implanted layers. In order to heat conveniently a large spectrum of metals and metallic alloys in vacuum and in the presence of plasma, as mandatory for efficient PIII, it is necessary to count on a stable heat source, able to provide steady temperatures in the range of 200 °C to more than 1000 °C. This has been accomplished in the current experiment by means of a thermionic cathode composed of a rolled tantalum foil covered with (Ba,Sr,Ca)O. Work-function of this electron source is around 2.1 eV, which is much lower than 4.5 eV of typically used tungsten filament. Metallic samples studied, in this case, are the anode of the discharge itself, being polarized during the heating cycle by positive DC voltages in the 100–800 V range. They are implanted with negative pulses up to 10 kV/300 Hz/40 μs.

© 2010 Elsevier B.V. All rights reserved.

1. Introduction

Plasma immersion ion implantation (PIII) has been shown to be an effective technique for surface modification of different types of materials. It has been successfully employed to modify the surface properties of semiconductors [1], polymers [2], metals [3] and metallic alloys [4]. For the case of metallic substrates, however, the thin modified layer produced by ion implantation is a constraint to be overcome, since thicker layers are more suitable to withstand severe wear, corrosion, etc. [5], in harsh environments.

One of the ways to achieve such thicker treated layers during PIII is to use hybrid processes, mainly combining PIII and deposition [5]. Nevertheless, adhesion problems and dimensional changes often associated with coatings [6] can be a drawback. In a pure PIII process, which circumvents such negative points, another alternative is the increase in temperature of the substrate during ion implantation [7,8]. In fact, it facilitates the thermal diffusion of ions into the bulk of the substrate. The thickness of the treated layer for this case can be increased easily to more than one order of magnitude greater than without heating.

In the PIII a substantial amount of thermal energy is transferred to the substrate due to the ions impinging on its surface. In most of the PIII systems control of the temperature of the substrate is achieved by varying the duty cycle of the pulsed voltage and its amplitude. In that way, temperature barely exceeds 400 °C, even using very high voltage

pulses and high repetition pulse rates. Such temperatures are sufficient to improve mechanical properties of materials that are not used in very high temperatures, as is the case with cold-work steel [9]. If necessary, additional temperature increase must be obtained with the help of auxiliary heating. Ueda et al. [10] performed high temperature PIII of Ti6Al4V samples by heating the sample holder to 800 °C, using a heated tungsten filament inside the holder. Fouquet et al. [8] used the technique of heating the whole PIII vacuum chamber to a temperature of 800 °C for the same purpose. Other heating mechanisms include the use of infrared lamps and boron nitride heater, in this case for post-annealing of nitrogen implanted stainless steel [11].

In this paper, a precise control of the temperature of the substrate in a wide range during PIII is accomplished by means of an electron source made of a thermionic cathode of (Ba, Sr, Ca)O. The aim of this manuscript is to describe, in details, the developed system, concerning the hardware, the electrical set-up, the characterization of the oxide cathode, explaining the way the temperature is controlled during PIII.

2. Hardware for high-temperature PIII

The experimental set-up used to perform high-temperature PIII can be seen in Fig. 1. In the scheme, the sample holder plays the role of the anode of the discharge itself, being positively polarized by DC voltages in the 100 to 800 V range in relation to the chamber wall that is grounded. The thermionic oxide cathode generates primary electrons to help with the breakdown of the glow discharge, which happens in a pressure range of 10^{-3} mbar, suitable for PIII. Electrons produced by the oxide cathode are drawn to the sample holder,

* Corresponding author. Tel.: +55 12 39456692; fax: +55 12 39456710.
E-mail address: rogerio@plasma.inpe.br (R.M. Oliveira).

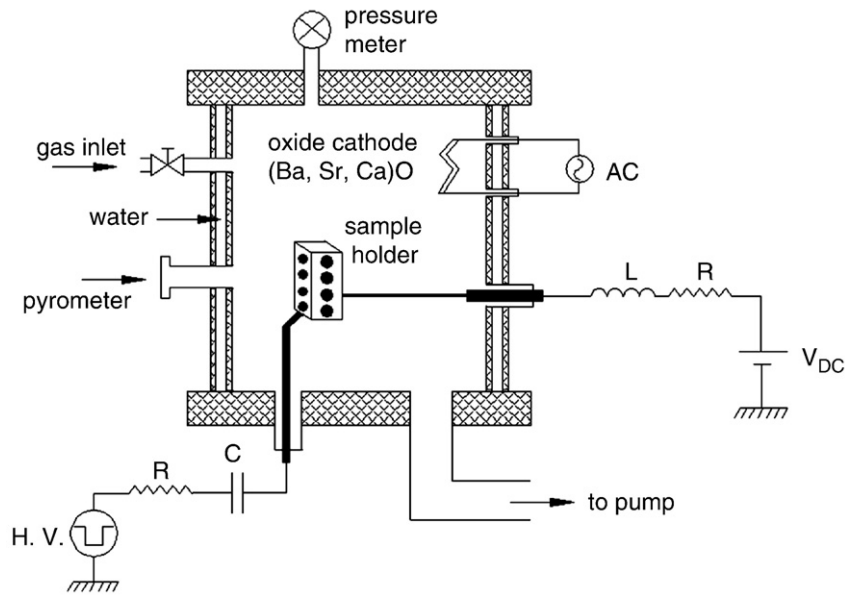


Fig. 1. Set-up for high-temperature PIII.

causing the heating of the samples. When high negative voltage pulses are applied to the samples, ion implantation takes place.

2.1. The electrical set-up

By analyzing the duty cycle of the waveform applied to the samples, as shown in Fig. 2, one can observe H.V. negative pulses floating on the positive DC level of the glow discharge, leading to ion implantation and heating of the samples, respectively.

Typical PIII performed in our experimental set-up runs with HV negative pulses at 300 Hz/40 μ s. It represents a duty cycle of 1.2% that has been used for ion implantation, customarily. With the new set-up, the remaining 98.8% of the time is used to heat up the samples.

The coupling between the outputs of the glow discharge power supply and of the HV pulser, both applied at the same time to the sample holder, was performed by using an external electrical circuitry, which equivalent circuit is shown in Fig. 3a. In this circuit, an inductor of high inductance L1 of 80 mH is placed between the current limiting resistor R1 of the glow power supply and the sample holder and 5 HV capacitors of small capacitance (5 kV/100 nF each) in series are put between the output of the HV pulser and the sample holder. The inductor was built by using 5 pairs of E-shaped ferrite

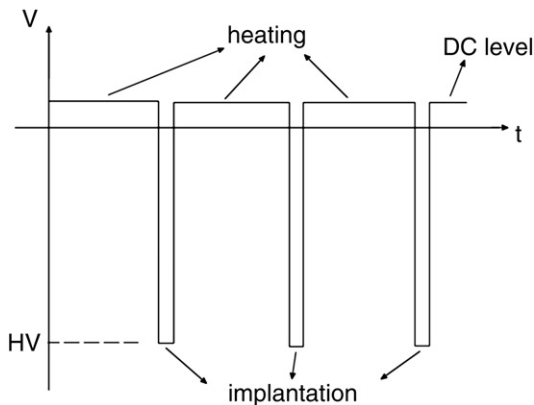


Fig. 2. Waveform of the potential applied to the sample holder.

cores to form 5 windings connected in series with 120 turns wound around each pair of cores. This inductance was measured using an LC bridge at AC frequencies of the order of 10 kHz. In this way the inductor avoids the HV pulse applied to the sample going into the DC power supply, while the total capacitance C1 of 20 nF blocks the application of the DC level into the HV pulser.

The plasma resistance is modeled by a fixed resistor R2 of 8 k Ω , which is calculated approximately by dividing the pulse voltage peak by the corresponding pulse current peak, and the plasma sheath by a very small capacitance C2 in parallel with this resistance. The respective waveforms simulated in the Spice simulator (Circuit Maker 2000) for the plasma voltage V and current I are shown respectively by the dotted curves in Fig. 3b and c and compared to their corresponding experimental results given by the solid lines. The experiments were performed applying HV pulse peak of 4 kV, pulse duration of 23 μ s, 250 Hz of pulse repetition rate, with a 500 V DC potential set for the glow discharge source. Notice that there is a reasonable agreement between the experimental data and the simulation results on the pulse flat-top. The output V/I drop observed on the waveforms is due to the RC discharge of the HV pulser through the plasma during the pulse application. As capacitor C1 is in series with the output of the HV pulser the equivalent RC time constant is decreased as C1 is lower than the pulser bank capacitance, which produces a higher voltage or current pulse drop. However, the main discrepancy on the comparison of waveforms appears to be during the $V-I$ inversions after the main pulse extinction. When the switch of the HV pulser switches-off, the plasma sheath extinguishes, being represented by the discharge of the capacitance C2 through the plasma resistance R2. Also, at this time, the voltage across R2 inverts as the capacitor C1 is still charged and the output of the HV pulser is grounded by the switch. Consequently, the plasma current follows the voltage inverting its signal since the plasma resistance is considered to be linear in the Spice model. Both the V/I experimental and simulated waveforms present similar shapes after the main pulse extinction, but in the case of the experimental current curve the peak is more pronounced probably because the value of the inductance in practice is much less than 80 mH since the ferrite cores work well at higher frequencies and the pulse repetition rate used in the experiment was of only about 250 Hz. Also note that the decrease in the simulated current after pulse inversion is smoother because of the higher value of

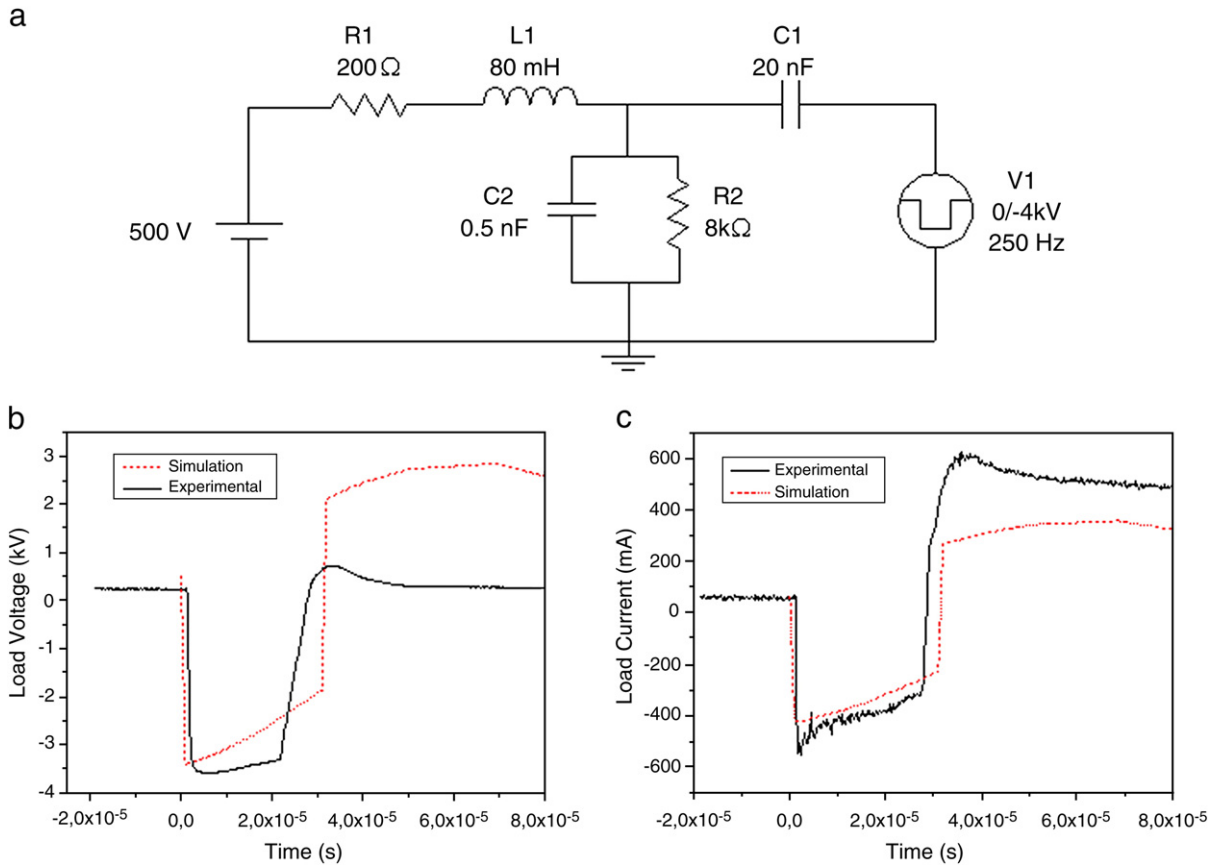


Fig. 3. a) Equivalent electrical circuit; load waveforms of: b) voltage and c) current.

inductance used in the Spice simulation. On the other hand, with the voltage waveforms, the experimental result shows that the inverted peak is very small because of the low effective inductance L1 in practice and due to the faster extinction of plasma sheath in the experiment. This is confirmed by the higher peak of the experimental plasma current with its rapid decrease rate observed (see solid line in Fig. 3c).

2.2. The oxide cathode

Oxide cathodes are simple and efficient electron emitters since they require low power consumption to perform electron emission, due to the low work-function of the oxide coating [12,13]. In this experiment, a (Ba,Sr,Ca)O was used to cover the inner side of a thin (0.001 in.) rolled tantalum foil, that emits electrons when it is ohmically heated. The foil was painted with a carbonate suspension. The chemical composition of the present coating was based on the ASTM-F270-56 T report for diodes [14], as follows: BaCO₃=57.2%, SrCO₃=38.8%, CaCO₃=4%, and a liquid phase composed of amyl acetate, ethyl alcohol and nitrocellulose.

A thermal degradation of the carbonates and of the nitrocellulose as well is necessary to get the oxide films. During this “activation process” large amounts of organic gases, such as CH₄, CO, CO₂ and NO_x are released. The graph of Fig. 4 shows the variation of the vacuum chamber pressure as function of cathode temperature during the carbonate conversion process. In the graph three peaks can be identified, at 475 K, 862 K and 1110 K, corresponding to the degradation of the nitrocellulose, strontium and barium carbonate, respectively. The degradation of the CaCO₃ was not detected, since a small amount of this substance was present in the coating.

The cathode can work in the voltage limited regime, in which electron emission is governed by Child–Langmuir law [12], or in the

temperature-limited regime, which electron emission is given by [14]:

$$J = \frac{\sqrt{2}e(2\pi mk^5)^{1/4}}{h^{3/2}} n_b^{1/2} T^{5/4} \exp\left(\frac{-\chi + \Delta\epsilon/2}{kT}\right) \tag{1}$$

where *e* and *m* are the electronic charge and mass, respectively, *k* is the Boltzmann's constant, *h* is Planck's constant, *T* is the cathode temperature (in Kelvin), *n_b* is the number of impurities level and $\chi + \Delta\epsilon/2$ is the true work-function. For this regime, suitable voltages

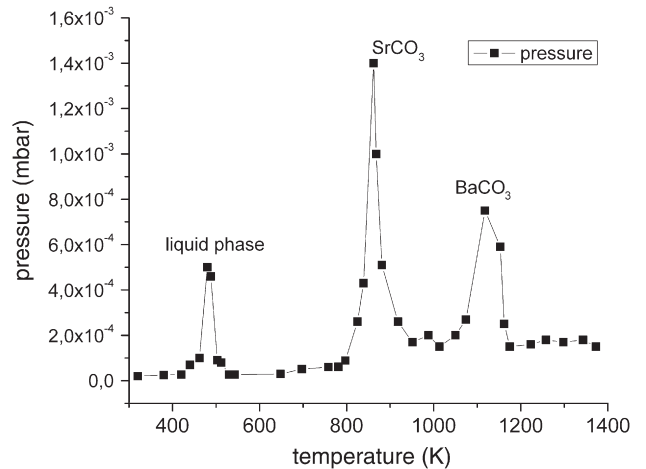


Fig. 4. Vacuum chamber pressure as a function of the temperature of the oxide coating during activation of the cathode.

were applied to the anode and thus the electron current density at the anode was recorded, as a function of the temperature of the oxide cathode. The slope of the fitting curve of the exponential region of the plot of $\ln J/T^{5/4}$, as shown in Fig. 5, resulted in a work-function of the oxide cathode of approximately 2.1 eV. This value is much lower than the one found for tungsten filament, of the order of 4.5 eV [15].

3. High-temperature PIII results

After being loaded with samples of carbon steel 1020, the sample holder was polarized by positive DC voltages in order to attract the electrons produced by the oxide cathode. The variation of the temperature of the samples, monitored by an optical pyrometer, in accordance with the applied voltage (V_A) and with the temperature of the oxide cathode (T_C) is shown in Fig. 6. As it was expected, higher sample temperatures were reached by higher values of V_A and of T_C . Nevertheless, the slope of all the curves for $V_A > 400$ V indicates that a saturation point for V_A was not attained. Even though sample temperatures as high as 1000 °C have been measured, it can be noted that a plateau was not attained, indicating that further temperature increments are possible. In fact, both the T_C and the V_A can be further increased up to 1100 K and 800 V, respectively. The increase in the former causes an exponential growth of the current density emitted by the oxide cathode; the increase in the latter implies an increase of the current density in accordance with $V^{3/2}$.

The sample temperature can be modified by the variation of the following parameters: V_A , T_C , the duty cycle of the applied voltage and the pressure of the discharge. Most important, however, is that the electron emission from the oxide cathode is extremely stable for a certain condition of operation of the process and, as a consequence, very stable sample temperatures are attained. A desired temperature in the range of 400–1000 °C can be rapidly reached mainly by means of accentuated variation of T_C or V_A ; afterwards stable sample temperatures are obtained when such parameters are set in a fixed value.

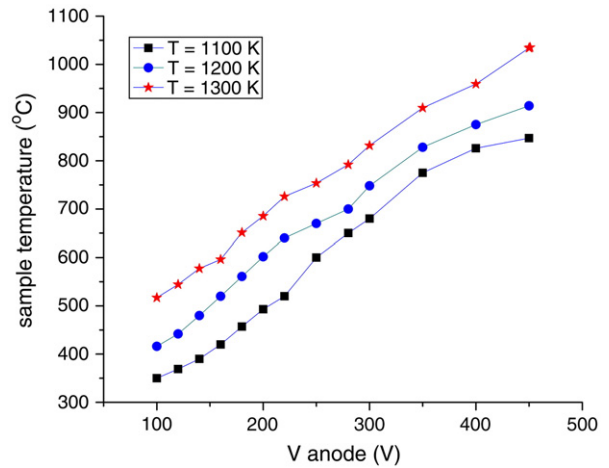


Fig. 6. Variation of the sample temperature as a function of the anode voltage and of the temperature of the oxide cathode.

4. Summary

The newly developed PIII system showed the possibility to perform high-temperature PIII processing by heating the samples by the bombardment of electrons thermionically produced by an oxide cathode. The work-function of the oxide coating of 2.1 eV was determined by operating the oxide cathode in the temperature-limited regime. Stable sample temperatures during PIII were obtained in a wide range (400–1000 °C), even though higher temperatures can be attained. Next experimental step concerns the treatment of metals and metallic alloys using the developed process. Since temperature is the most important parameter to promote ion diffusion during PIII, it is expected that thicker modified layers can be obtained on the surface of the treated metallic substrates.

Acknowledgments

The authors would like to thank Mr. Francisco Eugenio Donatelli de Figueiredo Costa for helping with the building of the electrical set-up.

References

- [1] X.B. Tian, P.K. Chu, Rev. Sci. Instrum. (2000) 2839.
- [2] D.R. McKenzie, K. Newton-McGee, P. Ruch, M.M. Bilek, B.K. Gan, Surf. Coat. Technol. 186 (1–2) (2004) 239.
- [3] X.B. Tian, Z.M. Zeng, B.Y. Tang, K.Y. Fu, D.T.K. Kwok, P.K. Chu, Mater. Sci. Eng. A 282 (1–2) (2000) 164.
- [4] R. Wei, T. Booker, C. Rincon, J. Arps, Surf. Coat. Technol. 186 (1–2) (2004) 305.
- [5] X.B. Tian, P.K. Chu, Rick Fu, S.Q. Yang, Surf. Coat. Technol. 186 (2004) 190.
- [6] A. Anders, Handbook of Plasma Immersion Ion Implantation & Deposition, John Wiley & Sons, New York, 2000.
- [7] L. Marot, M. Drouet, F. Berneau, A. Straboni, Surf. Coat. Technol. 156 (2002) 155.
- [8] V. Fouquet, L. Pichon, A. Straboni, M. Drouet, Surf. Coat. Technol. 186 (2004) 34.
- [9] G. Thorwarth, S. Mändl, B. Rauschenbach, Surf. Coat. Technol. 125 (2000) 94.
- [10] M. Ueda, M.M. Silva, C.M. Lepienski, P.C. Soares Jr., J.A.N. Gonçalves, H. Heuther, Surf. Coat. Technol. 201 (2007) 4953.
- [11] S. Mändl, R. Günzel, E. Richter, W. Möeller, B. Rauschenbach, Surf. Coat. Technol. 128–129 (2000) 423.
- [12] T.T. Forrester, Large Ion Beams: Fundamentals of Generation and Propagation, John Wiley, New York, 1988.
- [13] K.M. Poole, J. Appl. Phys. 26 (1955) 1176.
- [14] Relative Thermionic Properties of Materials Used in Electron Tubes. Tentative Method, for Test, ASTM-F270-56 T. American Society For Testing Materials (1956).
- [15] W.H. Kohl, Handbook of Materials and Techniques for Vacuum Devices, Reinhold, New York, 1967.

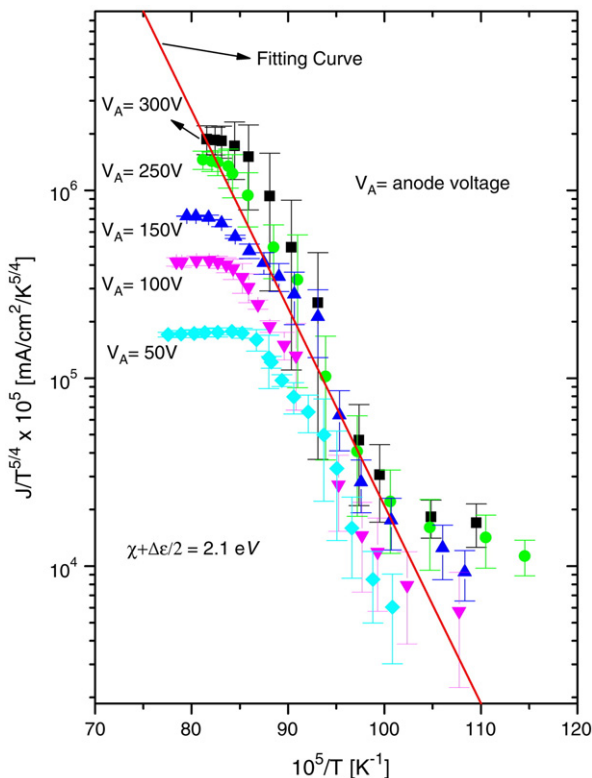


Fig. 5. Graph for the determination of the true work-function of the oxide cathode.